



Non-contact optical sensor to detect free flying droplets in the nanolitre range

J. Tröndle^{a,*}, A. Ernst^a, W. Streule^b, R. Zengerle^a, P. Koltay^{a,b}

^a Laboratory for MEMS Applications, Department of Microsystems Engineering (IMTEK), University of Freiburg, Georges-Koehler-Allee 106, 79110 Freiburg, Germany

^b BioFluidix GmbH, Georges-Koehler-Allee 106, 79110 Freiburg, Germany

ARTICLE INFO

Article history:

Received 23 July 2009

Received in revised form

12 December 2009

Accepted 17 January 2010

Available online 11 February 2010

Keywords:

Optical sensor

Non-contact detection

Nanolitre dispensing

Process control

Droplet detection

ABSTRACT

This paper reports on a non-contact optical sensor for the detection of single droplets in flight. The sensor allows for online process control of non-contact dispensing systems delivering droplets in the nanolitre range. A dispensed liquid droplet, which passes through the optical transducer, leads to a change of the light intensity caused by absorption, reflection and diffraction. The change in light intensity measured by a photo transistor provides information about, e.g. droplet size, velocity and shape. This information is encoded in the time dependent signal shape that yields a characteristic “fingerprint”-signal for each droplet. The fabrication of the sensor is achieved by standard printing circuit board (PCB) technology. Therefore, an easy adaption of the sensor to different kinds of contactless dispensing system and furthermore a very cost efficient production is granted.

© 2010 Elsevier B.V. All rights reserved.

1. Introduction

In the last decades the demand for microfluidic systems in MEMS technology has steadily increased following the trend of industrial products in general to become more and more miniaturized [1,2]. Nowadays, the most popular and commercially successful applications of microfluidic systems are ink-jet printers, which feature highly precise dispensing characteristics to provide the required printing resolution. For the liquid handling in pharmaceutical, biological and medical applications a precise and reproducible dispensing process is also of highest importance. Unfortunately, for such applications dispensing of droplets is much more difficult than for printing, because complex and widely varying liquids and bio-reagents have to be dispensed. Therefore, liquid-handling systems for life-science applications have not reached the stability and performance of printheads operating only with one type of ink. Thus, the control of the dispensing event is essential for fault detection like missing droplets, clogged nozzles or wrong liquid volume or type.

Control of droplet dispensing devices is often achieved by monitoring flow or pressure inside the dispensing device [3,4] or using optical cameras to image droplets in flight [5]. While the first approach mostly requires integration of a sensor into a specific dispensing device and calibration for a specific liquid, the latter suffers from the bulky size of the camera and the difficulty to apply the method to multi-channel systems. Therefore, this paper follows

the approach to detect dispensed droplets in flight on their way to the target. Such droplet sensors have been proposed for example earlier for counting droplets in the intravenous drop chamber of an infusion set [6], to seize rain droplets [7] or to monitor non-contact dispensing devices [8,9].

Amongst others capacitive and optical approaches have been successfully followed to detect droplets of different liquids and size. However, so far non-imaging optical system that can detect droplets in the range of several hundred microns size, i.e. in volume range of several nanolitre have not been reported in the literature. In this paper such an optical droplet sensor is presented for use with arbitrary liquids. It can be combined with any suitable non-contact nanolitre dispenser to establish fast online process control. In the following various approaches are presented that have been studied to establish a non-imaging optical sensor for the described purpose. Based on the most promising approach a sensor was designed and fabricated. Finally, the experimental characterization of the sensor has been performed using a PipeJet™-dispenser from BioFluidix GmbH to deliver the droplets [10,11].

2. Experimental investigation of different approaches

Four different optical sensor setups have been analyzed to find the most suitable approach for monitoring non-contact dispensing systems in general. The mainly considered requirements for the various approaches were: (1) to ensure a small distance from dispenser orifice to the target substrate, which affects the spatial resolution of the system strongly, and (2) high sensitivity of the

* Corresponding author. Tel.: +49 761 203 7148.

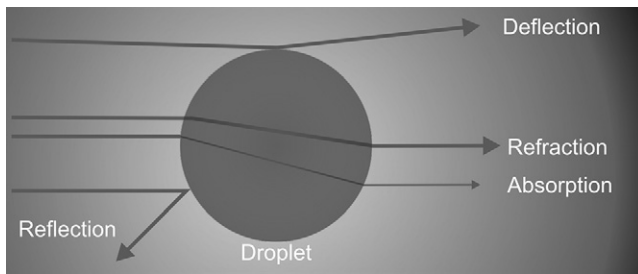


Fig. 1. Schematic of the interaction of a “large” droplet with a light beam.

generated analogue sensor signals with a high signal to noise ratio (SNR).

2.1. Working principle

The working principle of the presented sensor is based on the interaction of a free flying droplet with an infrared (IR) light beam. The intensity of the light becomes damped according to specific properties of the droplets media, e.g. absorption coefficient, refraction index etc. Such changes can be sensed by a light sensitive photo element, e.g. a photo transistor, which is positioned to detect the transmitted, scattered or diffracted light beam. Several different light scattering models are provided by literature which describe the effect of droplets or particles on light rays. Which of the theories holds for certain properties is related to the size of the scattering objects [12,13].

The minimum dispensing volume considered within this work $V_{\min} = 1$ nl, corresponds to a radius of $r = 62 \mu\text{m}$ for a single droplet. The working wavelength of the sensor is $\lambda = 950$ nm (for reasons that will be explained below). Thus, the smallest droplet is 65 times larger than the wavelength. Therefore, the interaction between droplet and light can be described in terms of geometrical optics [14]. A principle sketch of the interaction of a light ray with a “large” droplet is provided in Fig. 1. The basic effects can be described by refraction, reflection, absorption and deflection of the light ray.

Based on the described effects two basic ideas have been studied in this work. A first approach is to detect the light intensity which is reflected by an illuminated liquid droplet. A second approach follows the face to face detection of the luminosity of a light ray while a droplet passes through it. This approach depends on the decrease of the light intensity, which strongly relates to the absorption of the light, defined by the absorption coefficient of the droplets media.

The light absorption spectrum of water for example – which is one of the most prominent solvents in life-science applications – exhibits a local maximum in the near infrared (IR) spectrum [15]. Therefore, the working wavelength of the presented sensor is defined to be $\lambda = 950$ nm to generate the most significant optical absorption for water applications.

2.2. Sensor concepts and first results

The study of the four analyzed sensor approaches is described in the following. As active elements commercial light emitting diodes (LED) and photo transistors are used to realize the optical droplet detection.

2.2.1. Direct light measurement

The principle idea of this approach is to measure the decrease in a certain light intensity, caused by a droplet which passes by the light source. This approach is realized by the LED type (SFH 4010 from Osram) [16] and photo transistor type (PT 100 MF0MP1 from Sharp) [17], which were mounted below the dispenser nozzle facing each other to enable a direct detection of the emitted light, see

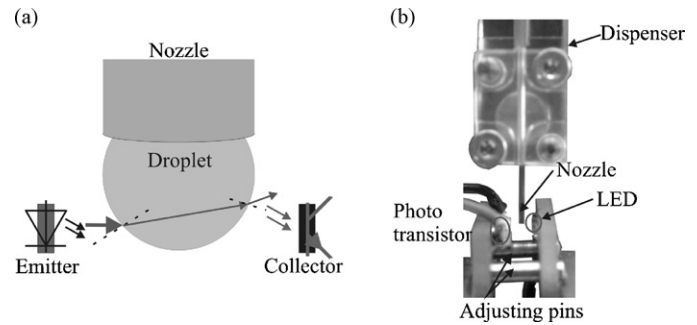


Fig. 2. (a) Schematic of the direct light measurement approach. (b) Photograph of the experimental setup.

Fig. 2. To identify the functionality of this approach, a first experiment was set up where each component was soldered on a separate printed circuit board (PCB). Two adjusting pins were used to align the active elements on the separate boards to each other. The mentioned components were chosen due to the LEDs wavelength at peak emission which is $\lambda = 950$ nm. The transistors peak sensitivity wavelength is $\lambda = 910$ nm, thus it provides a sensitivity of 95% at a wavelength of $\lambda = 950$ nm. Further the photo transistor provides a daylight filter. However, the signals show a detectable influence of ambient light. This influence can be detected by a shift in the sensor output voltage. At increased environmental illumination the shift in the analogue sensor signal increases as well. The signal shift can reach values up to $U_{\text{shift}} = \pm 100$ mV. However, the signal’s significance in terms of shape and amplitude (explained in the following, see Section 4), generated by the detection of a droplet, is not influenced by ambient illumination, which changes the initial output voltage only.

The distance between the LED and the photo transistor component as well as the nozzle position in vertical dimension, relative to the sensor components were manually adjustable. Each of the signals shown in Fig. 3 was generated by a single dispensed droplet with an average volume of $V = 15$ nl ($CV = 1.3\%$). To enable a simplified signal correlation to evaluate the significance of the certain sensor concept approaches, the signal offset has been fitted to zero by software.

The investigation of the influence of the nozzle distance relative to the sensor components has shown that the impact on the

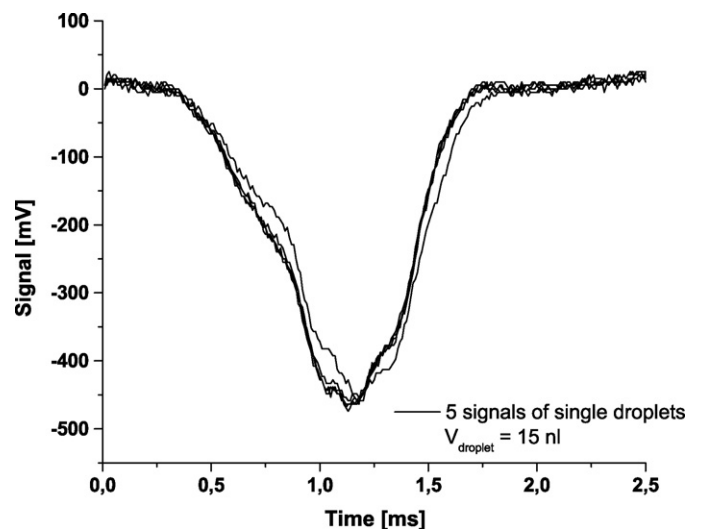


Fig. 3. 5 Signals recorded by the direct light measurement approach. LED to transistor distance $s = 2.65$ mm; single droplet volume $V = 15$ nl. Signal offset has been digitally fitted to zero.

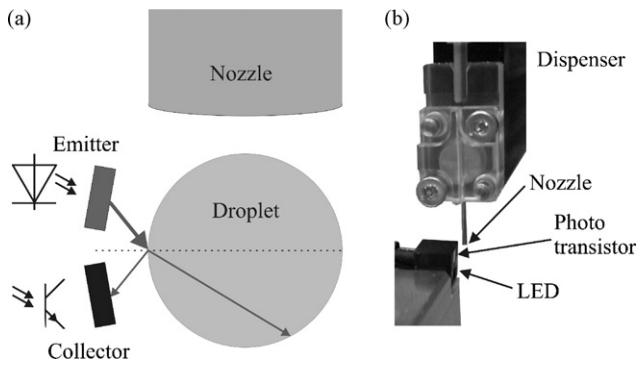


Fig. 4. (a) Schematic of the surface reflection setup, depicting the expected light path and (b) Experimental setup of the surface reflection approach.

significance of the generated signals is of minor importance. Therefore, the distance is defined by the component geometry only, thus the minimum nozzle to substrate distance can be set to 2 mm. The optimum distance between the LED and the phototransistor was experimentally determined to be $s = 2.65$ mm. This distance turned out to enable the generation of maximum signal amplitudes at the detection of passing droplets.

2.2.2. Surface reflection

The second approach is based on detecting the light intensity which is reflected from the surface of a droplet passing the sensor LED. For the realization of this setup a commercial reflective sensor device from Honeywell (HOA 1397-032) was used [18]. The working wavelength of this device is $\lambda = 935$ nm. A principle sketch of the approach and the implemented experimental setup are shown in Fig. 4.

The reflective sensor was aligned below the nozzle of the PipeJet™ dispenser. An ejected droplet passes the sensor where it becomes illuminated by the LED of the sensor. The phototransistor integrated within the sensor below the LED detects the reflected light. Due to the very low signal amplitudes and small SNR of the detected signals at droplet volumes from $V = 1$ nl to $V = 50$ nl, this approach was not investigated in more detail. This simple experiment is proof that standard reflection sensors designed for other purposes cannot be applied in a straight forward manner to sense droplets in the nanolitre range.

2.2.3. Inner reflection

This approach is based on the inner reflection of a light beam inside a droplet. A dispensed droplet will refract the light, emitted by the LED, in a way that it is bent towards the photo transistor. This light is supposed to generate a positive signal peak, allowing the detection of a single droplet in flight. The experimental setup to study this effect consisted of the two sensor components (SFH 4010 by Osram and PT 100 MFOP1 by Sharp) which were aligned sidewise at the orifice level of the PipeJet™ dispenser and facing towards the substrate as shown in Fig. 5. The big advantage of this approach would be the minimal distance from nozzle to substrate of less than 1 mm.

Relating to geometrical optics, three cases can be distinguished how a light beam propagates through a droplet. First it can enter the droplet, get reflected inside the droplet and then it exits the droplet in the direction of the sensor. This describes the ideal model for this approach. It is also possible that the light beam in the inner of the droplet becomes reflected more than once, which would lead to a further decrease of light intensity. Also the exit point of the beam can be different and hinder the detection of the reflected light. The third case considers total reflection inside the droplet. Once this occurs, it is impossible that the light beam will exit the droplet

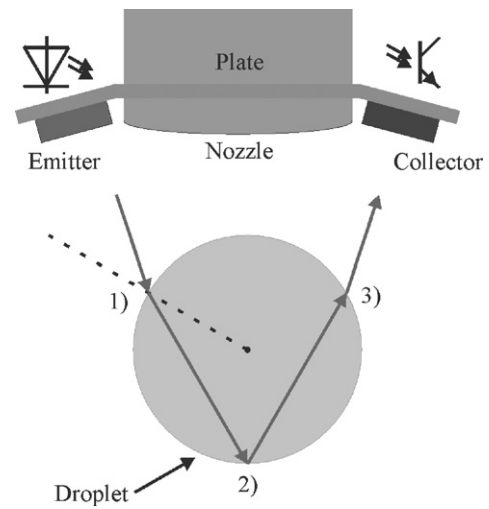


Fig. 5. Schematic of inner reflection setup.

again because of the law of regular reflection, which indicates that the angle of incidence equals the angle of reflection.

In the following only the first model is considered in detail because it is the most suitable for the droplet detection. However, also in this case one has to deal with a loss of intensity. This loss is caused by reflection and absorption. The opportunity of detecting a signal is generally low, but can be raised by high illumination intensity and the use of highly sensitive and low noise detectors. To achieve these requirements, lenses can be adapted to the LED, which focus the light ray to the flight path of the droplet. On the sensor side an amplification circuitry with an implemented filtering stage for the sensor signal can be realized.

The main issue in this context is not the absorption. The absorption of light intensity inside the droplet can be neglected, because assuming that the light beam would cross the droplet twice, the loss of intensity I is only 2% according to Beer's Law[19], see equation 1.

$$I = I_0 \times e^{-k \cdot x} \quad (1)$$

with I_0 being the intensity of the entering light beam, k being the absorbance of the material and x the thickness of the absorbing material.

The main reason for intensity loss within the droplet is given by Eq. (2) showing the balance of the transmitted part of light T and the reflected part R .

$$R + T = 1 \quad (2)$$

The reflected part R of the light can be calculated with Fresnel's law [20]. For this calculation a rectangular incidence of the light beam is assumed, where n_1 and n_2 are the indices of refraction for air and water with $n_1 = 1.003$ and $n_2 \sim 1.33$ at a wavelength $\lambda = 950$ nm.

$$R = \left(\frac{n_2/n_1 - 1}{n_2/n_1 + 1} \right)^2 \quad (3)$$

As depicted in Fig. 5 the light beam has to traverse 3 boundary layers between water and air. When the light beam hits the droplet at position (1) and enters the droplet, the intensity of the entering ray is still 98%, since only a small part of light is getting reflected. However, the major loss of intensity occurs at point (2), where only 2% of the incoming light is reflected. The transmission at the last boundary layer (3) is again 98%, such that in total only 1.92% of the original light intensity can reach the sensor.

In theory, the intensity of the light source and the sensitivity of the photo transducer used for experiments would not rule out such a small amount of reflected light to be detected. However, this

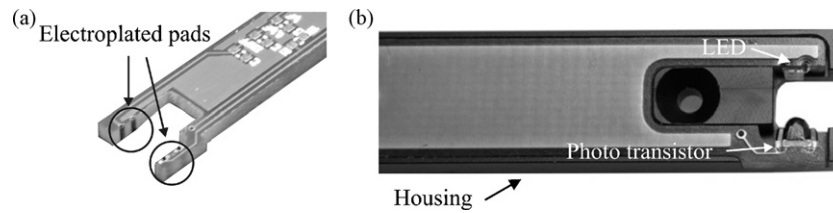


Fig. 6. (a) Electroplated through connections after the PCB-production process. (b) Optical sensor inside the developed housing.

approach did not lead to any significant experimentally detectable droplet signal, despite the fact that angle and position of the LED and photo transistor have been varied.

2.3. Selection of the preferred concept

The most significant and satisfying signals were achieved by the direct light measurement approach described in Section 2.2.1. It enabled a signal with significant analogue voltage at a reasonable SNR of better than 3, to be detected. Due to this promising results and the good feasibility, this setup was chosen for further evaluation. Based on the shown experimental results all alternative approaches have to be considered as less feasible.

3. Fabrication of the preferred concept

The sensor design for the direct light measurement approach features two separate hardware parts. One is the sensor board, which aligns the optical components (LED and phototransistor) to each other and, hosts the complete electronic circuitry to read the analogue sensor signals. The second part is the sensor housing, to precisely position the sensor below the dispenser unit with respect to the dispenser nozzle.

3.1. Design of the sensor board

A fundamental requirement to the final sensor size is to match the dispenser's lateral geometry (in the considered case this was PipeJet™ P9 dispenser by BioFluidix with 9 mm width). The experimental investigation in Section 2.2.1 resulted in an optimal inner gap size between the sensor components of $s = 2.65$ mm. Therefore, a forked sensor front was designed, which features vertical solder pads to populate the photo transistor and the LED at the inner edges of the fork at the defined distance, see Fig. 6(a). A printed circuit board (PCB) was designed and built to fabricate the complete sensor board. Here standard through connections (vias) were placed at the desired position at the forked front. A successive milling procedure opens the vias to enable the use of the inner, metalized surface as vertical soldering pads. Further it defines the accurate distance for the sensor components [21]. The outline dimensions of the finally populated sensor board were $8.5 \times 55 \times 2.6$ mm including the complete electronic read out circuit and components.

The LED is supplied with a constant current to provide an invariant intensity of the emitted light, in order that the sensor's performance is constant and the recorded signals become comparable. A signal shift due to temperature variations was not noticed during the test of the sensor. A two-channel operational amplifier is provided on board. One channel is used to enable a constant LED current, which can be adjusted by a resistive potentiometer, thus the emitted illumination intensity. The second channel is used for offset regulation of the sensor output voltage. This is realised by a standard differential amplifier circuit enabling the subtraction of an adjustable voltage from the sensor signal. The generated analogue signal is read out over a shunt resistor, connected to the measurement photo transistor. The acquired

signal does not require any further amplification or smoothing circuitry.

3.2. Design of the sensor housing

The major function of the sensor housing is to fix the sensor board at a well defined position relative to the nozzle. The prototype housing was fabricated using a stereo lithography process [22] and ended up in a outline geometry of $65.5 \text{ mm} \times 9 \text{ mm} \times 3.4 \text{ mm}$ ($L \times W \times H$) which exactly matches the geometry of the used PipeJet P9 dispenser. The axial alignment of the sensor and its location on the PipeJet™-module is realized with two countersink screws. The housing also provides a forked front side and follows the contour of the sensor board. Thus, the flight path of the dispensed droplets is not affected by the sensor. The sensor board is glued up side down into the housing, thus all the electrical components are embedded in the sensor housing, thus protected from short-circuits caused by wet contamination of the sensor, see Fig. 6(b).

Experiments have shown that the sensor signals are best reproduced if the distance of the sensor components to the orifice of the PipeJet™ dispenser is set to be 0.3 mm. This distance is added to the height of the blank sensor PCB of 1.6 mm, leading to a minimal distance from nozzle to substrate of 1.9 mm for the studied configuration.

4. Experimental results and signal analysis

The following section presents the experimental results obtained with the direct light measurement approach. The signals are analyzed with respect to the influence of different droplet properties like droplet volume and velocity. Purified water was used as liquid for all experiments.

4.1. Experimental setup

The experimental setup depicted in Fig. 7 was used to evaluate the performance of the sensor and the correlation between droplet properties and sensor signal. To generate the droplets a PipeJet™-

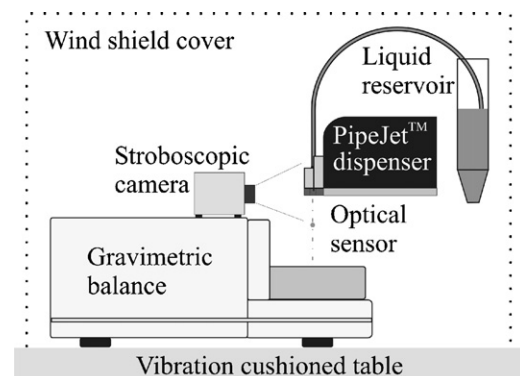


Fig. 7. Schematic of the used measurement setup and the used measurement technique.

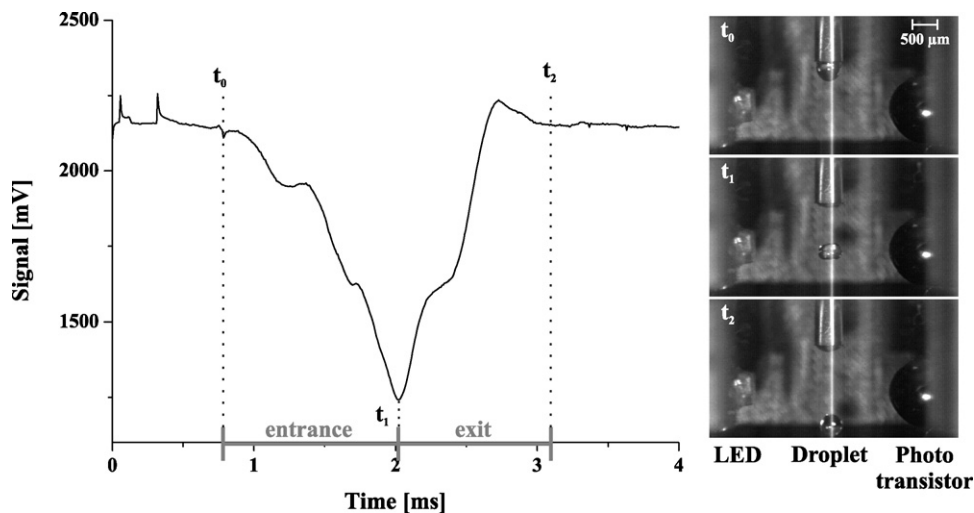


Fig. 8. Signal response (5 signals) and according stroboscopic images. (a) Droplet entrance into the sensor. (b) Droplet located in centre of the sensor. (c) Exit of the droplet.

P9 dispenser module was used. This direct displacement dispenser allows for the reproducible dispensing of droplets and further provides the option of changing the droplet volume and velocity in a wide range. Therewith it was possible to relate changes in the droplet properties to the changes in the sensor signal. To enable a detailed and precise investigation of the droplet characteristics like volume and velocity further equipment was used additionally to the optical sensor. A high precision balance [23] allowed for the accurate volume determination of the dispensed droplets. The balance features a resolution of $0.01 \mu\text{g}$ which enables an accurate single droplet volume determination in the focused range. The balance was installed on a vibration cushioned table and covered by a wind shield, see Fig. 7. With this setup the environmental influences on the balance are minimized, which is essential to attain accurate and reliable results. However, the balance is not suitable for the detection of dispensing irregularities like satellite droplets and to determine the droplet velocity. For that reason a stroboscopic camera setup was used to visualize the droplet in flight. Using the stroboscopic camera [24] the optical sensor signal could be correlated to the shape and the velocity of the dispensed droplet.

4.2. Signal characteristics

For the first experiments all droplets were dispensed with the same dispenser actuation parameters. The stroboscopic camera was triggered by the electronic driving unit of the PipeJet™-system. Thus, the sensor signal and the camera pictures have the same starting point, which allows for relating the stroboscopic pictures to the recorded signals. Due to the highly reproducible PipeJet™-dispensing process very similar sensor signals are generated (as can be seen in Fig. 8 where five consecutive signals are plotted, showing negligible variance).

The results as given in Fig. 8 show that the signal is divided into two sections. The first section between point (a) and (b) shows a decreasing voltage when the droplet enters the sensor. The sensor signal reaches its minimum when the droplet passed the half way through the sensor. Section two is characterized by the exit behaviour of the droplet out of the sensor. Here the sensor signal increases until it recovers to the original voltage level.

Characteristic properties of the signal are the positive overshoots at the start and the end of the negative peak. This can be explained by the refractive characteristics of the dispensed media. This phenomenon occurs mainly for spherically shaped droplets. The droplet depicted in Fig. 8 shows this overshoot very distinct at the exit of the droplet.

The dispensed droplet bends the illuminating light into the direction of the active area of the photo transistor. Therefore, the detected light intensity increases to a maximum. Due to the symmetric alignment of the sensor the overshoot, caused by reflection, is detected when the droplet enters as well as it leaves the sensor.

The steadily falling signal during the entrance and the steadily increasing signal during the exit of the droplet suggest that the droplet's shape did not change in a significant way, while passing through the sensor. The stroboscopic image sequence in Fig. 8 is proof that this is indeed the case.

4.3. Signal dependence on droplet volume

The parameter that influences the dispensed droplet volume produced by the PipeJet™ dispenser is termed stroke length [μm]. It determines the extension length of the piezo actuator. An increasing extension length goes along with increasing droplet volumes. In this section the influence of different droplet volumes on the sensor signal are examined.

Fig. 9 depicts three signals generated by three different sized droplets. It can be seen that higher dispensed volumes lead to larger negative signal peaks. The different droplet volumes lie in a range from $V = 13 \text{ nl}$ to $V = 47 \text{ nl}$. Comparing the signal width for the 13 nl and 47 nl signals, it turns out that the signal generated by the lower

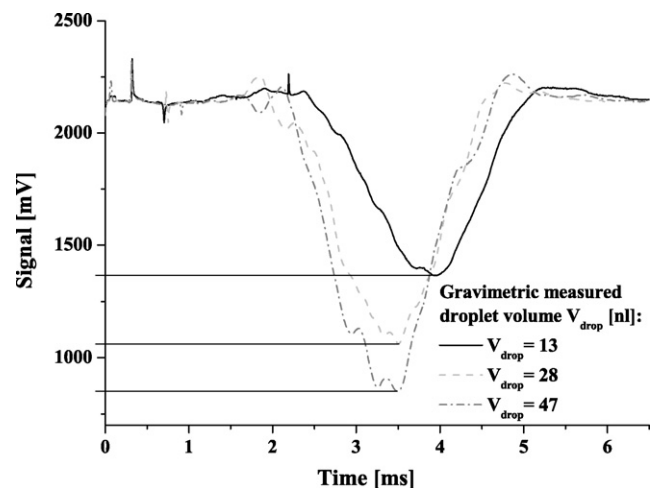


Fig. 9. Signals recorded for three different droplet volumes in a range of $V = 13\text{--}47 \text{ nl}$.

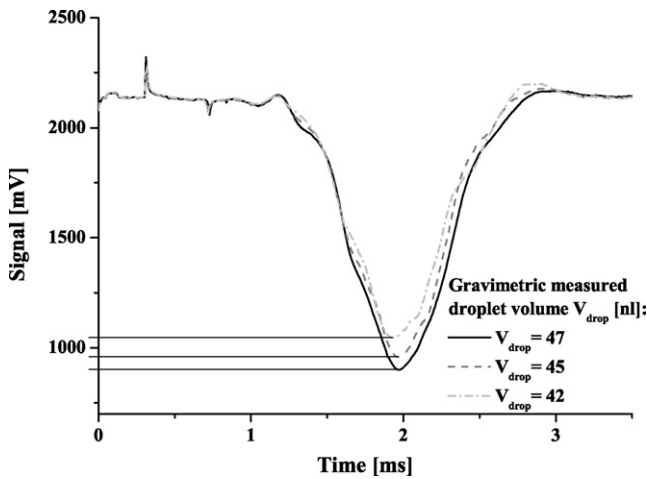


Fig. 10. Signals recorded for droplets in a volume range of $V=42\text{--}47$ nl.

volume droplet leads to a wider shape of the signal characteristics. This can be explained by a lower droplet velocity. Due to the lower stroke length, less momentum is transferred by the PipeJet™ dispenser’s piston to the liquid which leads to a lower volume as well as a smaller velocity of the ejected droplet (for more details see [11]). Furthermore it can be seen that for each droplet volume and its associated velocity the sensor signal has a characteristic shape which can be interpreted as a “fingerprint” being specific for the dispensing parameters (droplet volume, velocity, liquid type).

The sensitivity of the sensor was tested by recording signals in a range of stroke lengths from $23\ \mu\text{m}$ to $25\ \mu\text{m}$. The acquired signals are depicted in Fig. 10. The corresponding dispensed liquid quantities were in a volume range from 42 nl to 47 nl. As depicted in Fig. 10 a stroke length variation of $1\ \mu\text{m}$, thus a volume change of approximately 2 nl can be detected by a significant change of 60 mV in the signal.

To investigate the lower detection limit of the sensor the stroke length was reduced to the smallest value at which droplets were reliably dispensed. Fig. 11 shows the signals generated by droplets dispensed at a stroke length of $5\ \mu\text{m}$. The droplet volume of $V=3.8$ nl was gravimetrically determined. Even those small droplets lead to a signal peak of $U \approx 570$ mV and can be reliably detected due to the low noise characteristics of the sensor of about $U_{\text{Noise}} = 10\ \text{mV}_{\text{pp}}$. Given the high signal to noise ratio most likely even smaller droplets could be certainly detected, since the sensitivity of the sensor is at least $30\ \text{mV/nl}$, see Fig. 9. However,

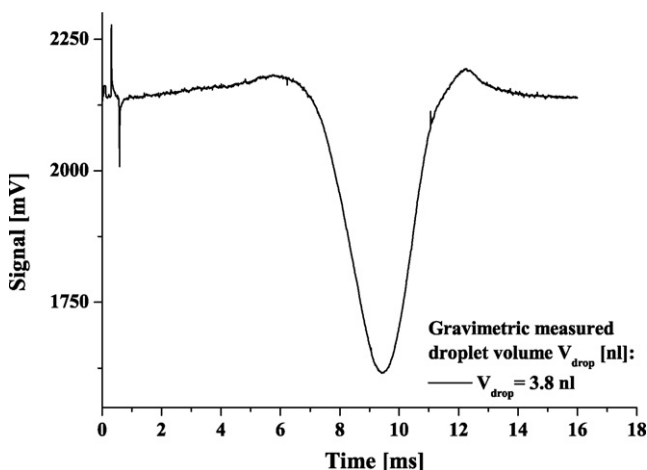


Fig. 11. (a) Signals acquired for single droplets with a volume of $V=3.8$ nl.

significance scales up with decreasing volume, caused by the non-linear coherence of droplet radius and droplet volume ($V=4/3r^3\pi$). Thus a droplet volume increase of 1 nl extends a 50 nl droplet by 2%, whereas a 10 nl droplet increases 10%.

The measurements have shown that the negative signal amplitude strongly depends on the droplet volume. Higher volumes generate larger negative amplitude while it decreases for smaller droplets. However, directly retrieving a quantitative value for the droplet volume was not possible. The sensor allows for the detection of a change in the droplet volume of $\Delta V=2$ nl like shown above, but it does not deliver quantitative information on the droplet volume. The detectable volume range experimentally defined for the presented sensor is 3.8–47 nl, dependent on the used dispensers volume range [11]. Further the signal width shows a dependency on the droplet velocity. Due to the longer exposure time to the sensitive sensor area, slow droplets generate wider signals than faster ones. The influence of droplet velocity and shape to the signal will be explained more detailed in the following chapter.

4.4. Signal dependence on droplet velocity

In the following section the impact of different droplet velocities and fluctuations in the droplet shape to the generated analogue sensor signals was studied. Therefore; droplets at different velocities were measured with the same experimental set up (see Section 4.1). The resulting signals of three significant samples are shown in Fig. 12, together with the corresponding stroboscopic images for each of the signals. Obviously increasing droplet velocity leads to a time shift of the signal, caused by the faster droplet approach to the sensor, thus the earlier entrance into the sensitive area. Furthermore, the signal width decreases with increasing velocity, while steeper slopes of the signal peak can be observed, see Fig. 12.

Fig. 12 also highlights the effect of droplet shape on the sensor signal. The stroboscopic image of the droplet with a velocity of $1.39\ \text{m/s}$ (determined from the stroboscopic images) shows a dispensed jet which splits into two single droplets. The corresponding signal shows two negative peaks which arise from the two several droplets. The first signal peak is generated by the main droplet and is similar to single droplet signals, wherein the second one is much smaller and wider, generated by the separated satellite. Thus, the sensor is obviously able to detect irregularities in the dispensing process, like satellites.

The correct interpretation of these results leads to the possibility to estimate the droplet velocity directly from the generated signals. Therefore, the droplet’s traveled distance in a certain time interval has to be estimated. The distance from the entrance of the droplet to the droplet position at which the major signal peak occurs was determined for the used setup to be $\Delta x = 780\ \mu\text{m}$ (Point of maximum intensity). Assuming that the major signal peak is always generated at this particular position relative to the sensor, the droplet velocity v_{drop} can be estimated by calculating the slope between droplet entrance and minimum sensor output, see Eq. (4). With Δx being the traveled distance, t_{min} being the time elapsed from its entrance until the signal has reached its minimum value. The droplet entrance is set to the point at which the recorded signal falls below the average sensor output. The estimated velocity is compared to the stroboscopically determined value in Fig. 13.

$$v_{\text{drop}} \approx \frac{\Delta x}{t_{\text{min}}} \quad (4)$$

4.5. Signal dependence on droplet media

In this section the influence of different media on the sensor signal is investigated. Three different media have been tested, featuring different absorption spectra and rheology (pure water,

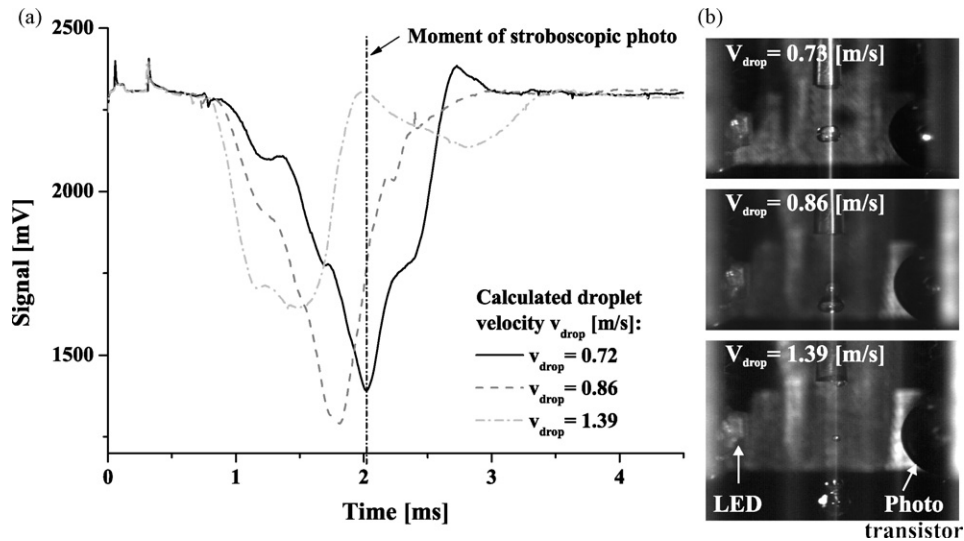


Fig. 12. (a) Signals recorded for single droplets with different velocities in a range of $v = 0.73\text{--}1.39$ m/s. (b) Stroboscopic images of the droplets; each recorded after $\Delta t = 2024$ μs .

ethanol and ink (75%). Due to the fact, that all media were aqueous solutions, they were dispensed with the same actuation parameters. This allows for dispensing droplets of almost equal volumes for each media, ejected by identical dispensing parameters, thus the signals become comparable. For the evaluation of the certain media influence to the sensor signal single droplets of $V = 10 \pm 1$ nl were dispense through the sensor.

Fig. 14 compares three single signals, generated by the different dispensed media. Beside small differences in the signal amplitudes ($V_{\text{diff}} = \pm 20$ mV) the signals show slightly variations in their characteristics, depict in the different smoothness and different shapes of the falling and rising edges. These signal variations might depend on the different media rheologies, which leads to variations in the shape of the different dispensed droplets and is not caused by the media itself.

5. Discussion

The signals, which are generated by the optical sensor, can be subdivided in an entrance and an exit phase. The sensor output decreases until the whole droplet volume is located inside the sensitive area of the sensor at the point of maximum intensity. Beyond this point, the droplet causes a rising of the sensor output to its ini-

tial voltage value until it has left the sensitive area, see Fig. 8. The evaluation of the stroboscopic images of a dispensing process has shown that the smoothness of the falling and rising edge depends on the fluctuations of the droplet geometry. The signal depicted in Fig. 8 shows very smooth signal edges generated by the almost spherically shaped droplets shown in the corresponding stroboscopic images.

Further the signal characteristic depends on the volume of the dispensed droplets. The correlation between volume and signal is depicted in Fig. 9. A higher droplet volume, leads to a higher negative signal peak. As described in Section 4.3, the signals are not suitable for a quantitative volume evaluation.

The measurement range of the sensor, evaluated in this work, is 1.5–71 nl and it provides a high volume sensitivity, which enables for the detection of volume changes of $\Delta V = 2$ nl. Theoretically the maximum detectable volume is only limited by the sensor geometry and would enable for detecting spherical droplets with diameters up to $d = 2.5$ mm.

Besides the influence of droplet geometry and volume to the signal, also the droplet velocity has an impact on the signal characteristics. A higher droplet velocity leads to an earlier entrance of the droplet into the sensor. Further the signal width decreases and the signal shows steeper slopes. As explained in Section 4.4 the droplet

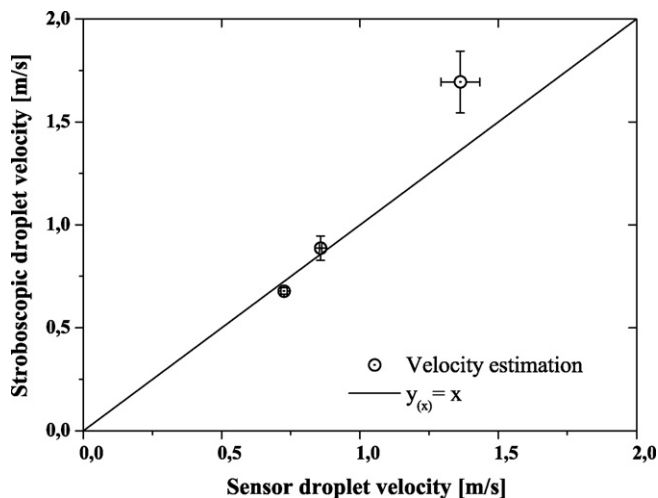


Fig. 13. Comparison of stroboscopic determined and estimated droplet velocity.

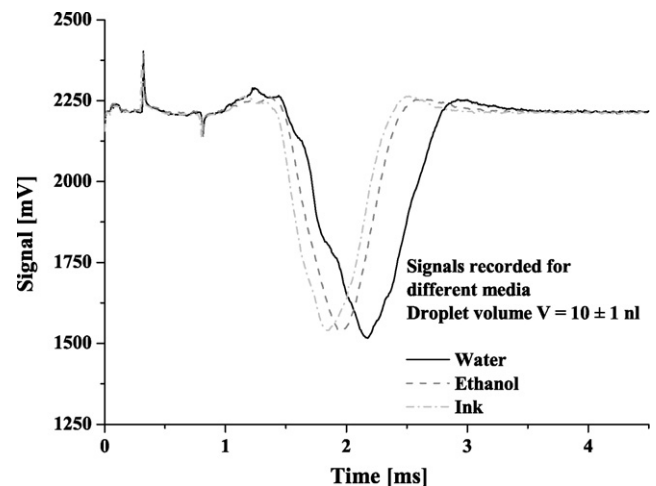
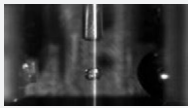
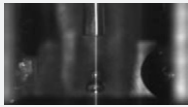
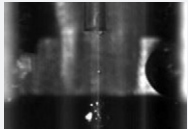


Fig. 14. Single droplet signals for water, ethanol and ink. The volume of each droplet is $V = 10 \pm 1$ nl.

Table 1

Illustration of three stroboscopic images for three different fast droplets, each recorded with a delay of $\Delta t = 2024 \mu\text{s}$ to the start of the signal recording. Comparison between the stroboscopic determined and the estimated droplet velocities.

Stroboscopic image ($\Delta t = 750 \mu\text{s}$)	v_{drop} [m/s] (stroboscopic)	v_{drop} [m/s] (calculated)
	0.68 ± 0.02	0.73 ± 0.01
	0.89 ± 0.06	0.86 ± 0.04
	1.69 ± 0.15	1.36 ± 0.07

velocity v_{drop} can be estimated by Eq. (4). A comparison between the calculated and the stroboscopic determined droplet velocities is given in Table 1.

Also irregularities like jets, satellites and the absence of a droplet can be detected by the presented sensor. As depicted in Fig. 12, dispensed satellite droplets can be detected as a successive signal peak after the main signal. This information enables to estimate whether the dispensing parameters are well adjusted to generate single droplet without irregularities like satellites.

Further, the comparison of the measurement of different media has shown that the presented sensor features a media independent measurement method.

6. Conclusion

The presented optical droplet sensor enables the user to detect the presence and absence of a free flying droplet in the nanolitre volume range. Although the signal does not allow for a quantitative droplet volume evaluation, it is highly sensitive to the droplet size. Changes in the dispensed volume of $\Delta V = 2 \text{ nl}$ can be identified by changes in the negative signal amplitude. The study in this work has further shown the impact of droplet shape and velocity on the signal.

Almost spherical shaped droplets generate very smooth slopes of the signal while fluctuations in the droplets shape result in sinusoidal characteristics in the falling and rising slope. Also irregularities in the dispensing process, like satellites which indicate harsh dispensing parameters, can easily be detected by the sensor.

The effect of droplet velocity to the signal is a narrowing of the signal and therewith an increased steepness of the rising and falling signal edge. According to this steepness the droplet velocity can be estimated from the signal.

So the sensor presented in this work is able to deliver “fingerprint”-signals for droplets in the nanolitre range, which provide minimum qualitative information about droplet shape, volume and velocity. Beside the high reproducibility of the signals and the high sensitivity of the signal to changes in the droplet characteristics ($S_{\text{min}} = 30 \text{ mV/nl}$), explained in Section 4, the sensor features an instantaneous read out, thus it can be utilized for online process control of non-contact dispensing systems. This can be realized by comparing each sensor signal to a given reference by calculating their correlation coefficients. Changes in any droplet parameter (volume, velocity or shape), thus changes in the signal characteris-

tics would entail deviations in the correlation coefficient, which can easily be detected. An experimentally defined threshold enables a semi-quantitative evaluation of a dispensing process. Signals leading to correlation coefficient below the threshold can be taken as hint for a defective dispensing process.

Acknowledgement

The authors are thankful to BioFluidix GmbH for the provision of the PipeJet™ dispenser and the necessary equipment and know how.

References

- [1] J. Comley, Continued miniaturisation of assay technologies drives market for nanolitre dispensing, in: Drug Discovery World Summer 2004, 2004, pp. 1–8.
- [2] Vermes Technik GmbH & Co., KG Palnkamerstraße 18–20 83624 Otterfing, <http://www.vermes.com>.
- [3] Seyonic SA Rue du Puits-Godet 12 2000 Neuchâtel, <http://www.seyonic.com/techflowsensor.php>.
- [4] P. Cooley et al., Application of ink-jet printing technologies to BioMEMS and Microfluidic systems, SPIE Conference on Microfluidics and BioMEMS 2001.
- [5] K. Thurov, T. Krüger, Volumenbestimmung kleiner Tropfen in der Nanodosierung, GIT Labor-Fachzeitschrift 2008, pp. 964–966.
- [6] H. Brown, W. Barnes, Apparatus and method for measuring drop size in an intravenous drop chamber, US Patent, US 6,562,012 B1 (2002).
- [7] W.P. Winn, An electrostatic theory for instruments which measure the radii of water drops by detecting a change in capacity due to the presence of a drop, Journal of Applied Meteorology 7 (1968) 929–937.
- [8] A. Ernst, A capacitive sensor for non-contact nanolitre drop detection, Sensors and Actuators A: Physical (2009).
- [9] W. Streule, Kontaktfreie und medienunabhängige Volumenbestimmung in Nanoliter Dispensern, Mikrosystemtechnik-Kongress 2005.
- [10] BioFluidix GmbH Georges-Koehler-Allee 106 79110 Freiburg, <http://www.Biofluidix.de>.
- [11] W. Streule, et al., PipeJet A Simple disposable dispenser for the nanoliter- and microliter range, JALA 9 (2004) 300–306.
- [12] G. Mie, Beiträge zur Optik trüber Medien, speziell kolloidaler Metallösungen, Annalen der Physik 25 (1908) 377–445.
- [13] E. Hecht, Optik, 3rd ed., Oldenburg Wissenschaftsverlag GmbH, München, Germany, 2001, ISBN:3-486-r24917-7, pp. 138–140.
- [14] W. Zinth, U. Zinth, Optik: Lichtstrahlen–Wellen – Photonen, 1st Ed., Oldenburg Wissenschaftsverlag GmbH, München, Germany, 2005, ISBN:3-486r-r27580-1, pp. 67–68.
- [15] G.M. Hale, M.R. Query, Optical constants of water in the 200-nm to 200- μm wavelength region, Applied Optics 12 (1973) 555–563.
- [16] Osram GmbH, Hellabrunner Straße 1, 81543 München, <http://catalog.osram-os.com/catalogue/catalogue.do?favOid=00000010000e500002003a&act=showBookmark&catId=EN&lang=en>.
- [17] Sharp Electronics (Europe) GmbH, SonninstraÙe 3, 20097 Hamburg, <http://www.sharpsme.com/Page.aspx/europe/en/part/PT100MF1MP1/>.
- [18] Honeywell International Inc., Product Page HOA 1397-032, http://sensing.honeywell.com/index.cfm?ci_id=140301&la_id=1&pr_id=152792.
- [19] A. Beer, Bestimmung der Absorption des rothen Lichts in farbigen Flüssigkeiten, Annalen der Physik und Chemie 86 (1852) 78–87.
- [20] M. Born, E. Wolf, Principles of Optics: Electromagnetic Theory of Propagation, Interference and Diffraction of Light, 7th ed., Cambridge University Press, Cambridge, United Kingdom, 1999, ISBN:0-521r-r64222-1, pp. 40–45.
- [21] Beta Layout GmbH, Im Aartal 14, 65326 Aarbergen, <http://www.pcb-pool.com/>.
- [22] robotmech Rapid Prototyping Stössl GmbH, Bundesstraße 11, 6842 Koblach, <http://www.robotmech.com/stereolithografie.html>.
- [23] Sartorius AG, Weender Landstraße 94-108, 37075 Goettingen, <http://www.sartorius.de/>.
- [24] VISIT GmbH & Co. KG, Postfach 6628 D-97016 Würzburg, <http://www.visit-gmbh.de>.

Biographies

Julien Tröndle was born in Freiburg, Germany in 1984. He received the diploma degree in medical engineering in 2008 from the University for Applied Science of Furtwangen, Campus Schwenningen. The topic of his work was the development of a process control for nanolitre dispensing systems by optical detection. This work was realized at the Laboratory for MEMS Applications, Department of Microsystems Engineering (IMTEK), University of Freiburg.

Andreas Ernst was born in Bad Säckingen, Germany in 1976. He received the diploma degree in medical engineering in 2006 from the University for Applied Science of Furtwangen, Campus Schwenningen. Currently he is working towards the PhD degree at the Laboratory for MEMS Applications, Department of Microsystems Engineering (IMTEK), University of Freiburg. His research interest includes

the development of direct quality control systems for pipetting- and non-contact dispensing systems.

Wolfgang Streule obtained his graduate in civil engineering in microsystem technology in 2003 at the University of Freiburg, Germany. From 2004 to 2007 he was working as a PhD student at the laboratory for MEMS Applications of the Institute of Microsystem Technology (IMTEK) for the further evaluation and optimization of the PipeJet™ technology. In 2007, he joined the BioFluidiX GmbH to continue the development of the PipeJet™ dispensing devices and dispensing platforms.

Roland Zengerle is the director of the Department of Microsystems Engineering (IMTEK) at the University of Freiburg, Germany. He also heads the Laboratory for MEMS Applications at IMTEK and in addition he is a director at the Institute for Micro- and Information Technology of the Hahn-Schickard-Gesellschaft (HSG-IMIT). HSG-IMIT is a non-profit organisation supporting industries in development of new products based on MEMS technologies. The research of Dr. Zengerle is focused on microfluidics and covers topics like miniaturized and autonomous dosage systems, implantable drug delivery systems, nanolitre and picolitre dispensing, lab-on-a-chip

platforms, tools for research on cells, thermal sensors, miniaturized fuel cells as well as micro- and nanofluidics simulation. Dr. Zengerle co-authored more than 300 technical publications and 30 patents. He is the European editor of the Springer Journal of Microfluidics and Nanofluidics. Dr. Zengerle serves on the international steering committee of the IEEE-MEMS conference as well as on the technical program committees of several other international conferences.

Peter Koltay studied physics at the Universities of Freiburg (Germany) and Budapest (Hungary) and obtained his PhD from the University of Freiburg in 1999. Afterwards he joined the laboratory of Prof. Zengerle at the Institute for Microsystem Technology (IMTEK) of the University of Freiburg as a faculty member. In 2005 he founded the company BioFluidiX GmbH to commercialize non-contact dispensing technologies developed at IMTEK. His research interests are especially related to the development of non-contact liquid-handling technologies, sensors for droplet detection and quality control, modelling of droplet and bubble dynamics, design and fabrication of passive direct methanol fuel cells and simulation of microfluidic devices by numerical methods.